



Investigation of Refractory Black Carbon-Containing Particle Morphologies Using the Single-Particle Soot Photometer (SP2)

Arthur J. Sedlacek, III,¹ Ernie R. Lewis,¹ Timothy B. Onasch,^{2,3}
 Andrew T. Lambe,^{2,3} and Paul Davidovits³

¹*Biological, Environmental and Climate Sciences Department, Brookhaven National Laboratory, Upton, New York, USA*

²*Aerodyne Research Inc., Billerica, Massachusetts, USA*

³*Department of Chemistry, Boston College, Chestnut Hill, Massachusetts, USA*

An important source of uncertainty in radiative forcing by absorbing aerosol particles is the uncertainty in their morphologies (i.e., the location of the absorbing substance on/in the particles). To examine the effects of particle morphology on the response of an individual black carbon-containing particle in a Single-Particle Soot Photometer (SP2), a series of experiments was conducted to investigate black carbon-containing particles of known morphology using Regal black (RB), a proxy for collapsed soot, as the light-absorbing substance. Particles were formed by coagulation of RB with either a solid substance (sodium chloride or ammonium sulfate) or a liquid substance (dioctyl sebacate), and by condensation with dioctyl sebacate, the latter experiment forming particles in a core-shell configuration. Each particle type experienced fragmentation (observed as negative lagtimes), and each yielded similar lagtime responses in some instances, confounding attempts to differentiate particle morphology using current SP2 lagtime analysis. SP2 operating conditions, specifically laser power and sample flow rate, which in turn affect the particle heating and dissipation rates, play an important role in the behavior of particles in the SP2, including probability of fragmentation. This behavior also depended on the morphology of the particles and on the thermochemical properties of the non-RB substance. Although these influences cannot currently be unambiguously separated, the SP2 analysis may still provide useful information on particle mixing states and black carbon particle sources.

INTRODUCTION

Black carbon (BC) is of interest to the climate change community because of its large positive contribution to radiative forcing, being second only to CO₂ in this regard (Ramanathan and Carmichael 2008; Bond et al. 2013). The ability of a BC-

containing particle to absorb solar radiation is determined primarily by the amount and optical properties of the BC component, but is also affected by other, non-BC components. These non-BC substances may have been present since particle formation or may have been collected subsequently, either by coagulation with other particles or through condensation of gaseous components. The optical properties of a BC-containing particle are strongly dependent upon particle morphology, i.e., particle shape and the location of the BC component within (or on) the particle. Due to the complex interplay among these various factors, and the changes that they may undergo during the lifetime of the particle, a quantitative understanding of BC radiative forcing has been difficult to obtain. In particular, one of the issues limiting further understanding has been the capability of obtaining real-time, *in situ* measurements of the morphology of BC-containing particles.

The Single-Particle Soot Photometer (SP2, Droplet Measurement Technologies; Schwarz et al. 2006; Moteki and Kondo 2007; Subramanian et al. 2010) is an instrument that measures, *in situ*, the time-dependent scattering and incandescence signals produced by individual BC-containing particles as they travel through a continuous-wave laser beam. Any particle traversing the laser beam will scatter light, and the BC component of a BC-containing particle will absorb some of the laser energy until its temperature is raised to the point at which it incandesces (hereafter we adopt the standard terminology of the SP2 community and denote any substance determined by the SP2 to be BC as refractory black carbon (rBC)). The scattering signal provides information on particle size, and the incandescence signal is used for counting rBC-containing particles and yields the mass of the rBC component within each particle (obtained via calibration). Hence, the SP2 can determine size-resolved number and mass concentrations of rBC-containing particles and thus provides information on the rBC particle population-based mixing states within ambient

Received 30 December 2014; accepted 9 June 2015.

Address correspondence to Arthur J. Sedlacek, III, Biological, Environmental & Climate Sciences Department, Brookhaven National Laboratory, Building 185E, Upton, NY 11973-5000, USA. E-mail: sedlacek@bnl.gov

aerosols. In addition, SP2 scattering and incandescence signals have been used recently to estimate the amount of the non-rBC component and infer the structure of individual rBC-containing particles, therefore suggesting the possibility that this instrument can also provide information on the morphology of rBC-containing particles (Sedlacek et al. 2012).

The amount of non-rBC material associated with an rBC-containing particle can be estimated by two different methods, both of which assume a core-shell configuration, in which a spherical rBC core is surrounded by a uniform concentric shell of non-rBC material, and both require assumptions regarding the densities and refractive indices of the rBC and non-rBC substances comprising the particle. The “leading edge optimization” (LEO) method (Gao et al. 2007; Moteki and Kondo 2008; Schwarz et al. 2008) is based on the temporal behavior of the scattering signal and on the peak magnitudes of the scattering and incandescence signals. The scattering signal will initially increase as the particle enters the laser beam, exhibiting a Gaussian dependence with time (following the spatial profile of the laser intensity, which the particle transits at constant speed). The magnitude of this signal will attain a maximum value and eventually decrease as the particle becomes smaller due to evaporation of the non-rBC substance, the energy absorbed by the rBC being dissipated as latent heat of this non-rBC material and by diffusion to the surrounding atmosphere. The initial portion of the time-dependent scattering signal (i.e., before any appreciable evaporation of the non-rBC material has occurred) is fitted to a Gaussian, yielding an estimate of the original optical diameter of the particle. This quantity, together with the rBC mass (which is obtained from the peak magnitude of the incandescence signal), can be used to determine the mass of the non-rBC material. Under the core-shell assumption, the amount of the non-rBC material can also be quantified as a coating thickness.

The “lagtime” method (Moteki and Kondo 2007; Subramanian et al. 2010) employs the temporal behaviors of both scattering and incandescence signals. The lagtime ($\Delta\tau$) is defined as the difference in the time of the peak in the (abrupt) incandescence signal, which occurs when all non-rBC material has been removed and the temperature of the rBC has risen to the point where it incandesces, and the time of the maximum value of the scattering signal. This quantity provides a proxy for the amount of non-rBC material – a greater lagtime indicating a larger amount of substance that must evaporate before the remaining rBC can incandesce (Schwarz et al. 2006; Moteki and Kondo 2007). This approach has been used to categorize rBC-containing particles as either aged or fresh, the two extremes relating to the amount of time since the production of the particle, and thus the amount of condensation of non-refractory material that has occurred (e.g., Subramanian et al. 2010).

It had been typically assumed that the SP2 lagtime should always be greater than or equal to zero for a core-shell configuration, as any non-rBC substance must evaporate before the

rBC can attain a sufficient temperature to incandesce (and sublimate), after which no material remains to produce any scattering signal. However, Moteki and Kondo (2007) observed negative lagtimes (i.e., the maximum value of the scattering signal occurring *after* incandescence) in a laboratory study involving rBC particles known to be in a core-shell configuration (having been formed by condensation of gases on a nearly spherical soot core) with a large amount of non-refractory material. They hypothesized that these negative lagtimes resulted from particle fracturing when the rBC could not dissipate the absorbed heat sufficiently rapidly to the non-rBC substance. This fracture would allow some of the remaining non-rBC material to pass through the laser and produce a scattering signal after the rBC had incandesced.

Sedlacek et al. (2012) observed negative lagtimes for a large fraction of ambient rBC-containing particles in some air masses. However, some of these particles, unlike those in the previous laboratory measurements, did not appear (based on the optical diameter method) to have large amounts of non-rBC material. These investigators concluded that the negative lagtimes occurred for particles for which the rBC component was at or near the surface. In particular, biomass-burning plumes were found to contain high fractions of such particles in several field studies, suggesting that this fraction could be used for source attribution. Other investigations (Dahlkötter et al. 2014; Moteki et al. 2014) have subsequently reported similar observations; for example, Moteki et al. (2014) reported that the fraction of ambient BC-containing particles in Tokyo with rBC near the surface of the particle was typically less than 10% but increased to near 40% in some cases. The conclusion that these observations result from BC being at the surface of the particles, and which is based on the temporal behavior of the scattering and incandescence signals observed for apparently different rBC-containing particle morphologies, may have important implications on the global radiative forcing by BC-containing particles, especially those from biomass burning.

In their work, Moteki et al. (2014) described a third approach, a new SP2 mixing analysis methodology that utilizes the behavior of the time-dependent scattering cross section to classify the particle morphology type. This method uses aspects from both the LEO and the lagtime approaches, and employs three quantities: the measured scattering cross section of the particle prior to evaporation (i.e., as it first enters the laser beam), the measured scattering cross section at the start of incandescence, and an independently calibrated scattering cross section of uncoated rBC. The ratio of the first two quantities provides information on particle evaporation; a ratio near unity implies that there is limited thermal contact between the absorbing rBC component and non-refractory component, and thus limited evaporation (what they refer to as “attached type”), whereas at the other extreme, a ratio much less than unity implies that there is greater thermal contact, such as what would be expected for a core-shell configuration (what

they refer to as “coated type”). The ratio of the scattering cross section of the particle prior to evaporation to the scattering cross section of the rBC alone quantifies the amount of non-rBC material and is used to define a range of conditions where particle morphology can be inferred from the first ratio. Direct comparisons between this new methodology and the lagtime approach have not yet been conducted; however, both methods provide mechanisms for inferring particle morphology based on the time-dependent behavior of the light scattered by rBC-containing particles relative to the rBC incandescence signal.

The current manuscript explores the utility of the lagtime method to infer particle morphology by conducting a systematic series of laboratory experiments to measure the SP2 scattering and incandescence signals from rBC-containing particles with different known morphologies and chemical compositions. Specifically, laboratory particles were generated containing rBC and either an inorganic salt or an organic substance, and with the rBC either on the surface, via coagulation, or as the core of a core-shell configuration, via condensation. In addition, the SP2 scattering and incandescence signals measured from particles of these types were investigated as a function of the SP2 operating conditions, i.e., laser power and sample flow rate.

EXPERIMENTAL DETAILS

In all experiments, atomized Regal black (RB, Cabot Corp), which has a compact, aciniform solid structure, was used for the rBC component and was chosen as a surrogate for collapsed soot. Scattering and incandescence signals from individual particles were measured with an eight-channel SP2 (revision D). The mass of the rBC contained in a particle is determined from the peak magnitude of the incandescence signal by calibration with RB, and is reported as a mass-equivalent diameter ($D_{me,rBC}$) based on an assumed density of 1.8 g cm^{-3} . The SP2 can detect incandescence signals from particles with $D_{me,rBC}$ in the range of ~ 70 – 600 nm , but scattering signals only from particles with initial diameters in the range of ~ 175 – 350 nm .

Particle number concentrations were measured with a condensation particle counter (CPC), and particle mobility distributions were measured with a scanning mobility particle sizer (SMPS). Sample preparation conditions (i.e., solute concentrations, etc.) were chosen to maximize the number of particles

with sizes within the detection range of the SP2 scattering channel to facilitate the utilization of the lagtime technique.

In the first set of experiments, lagtimes were determined from SP2 scattering and incandescence signals from particles formed by coagulation of RB with sodium chloride (NaCl; hereafter referred to as SC) and by coagulation of RB with ammonium sulfate ($(\text{NH}_4)_2\text{SO}_4$; hereafter referred to as AS), forming RB+SC and RB+AS particles, respectively. As both of these particle types are aggregates composed of two solid substances, they clearly cannot possess core-shell configurations. Both SC and AS were used because these substances have different thermochemical properties such as melting point, thermal diffusivity, specific heat, vapor pressure, and latent heat, and differences in these quantities would be expected to affect the rate and amount of intra-particle heat transfer and thus the lagtime behavior. For example, the melting point of AS (235°C) is much lower than that of SC (800°C), and its specific heat at 300 K ($188 \text{ J mol}^{-1} \text{ K}^{-1}$) is much greater than that of SC ($50 \text{ J mol}^{-1} \text{ K}^{-1}$). It should be noted that although in many techniques (such as thermal volatility) SC is considered to be refractory, in the present context it is considered to be a non-refractory substance.

The particle generation and sampling systems used for these measurements are shown in Figure 1. RB, SC, and AS were generated separately by atomization from aqueous solutions and then dried with an annular diffusion drier packed with molecular sieves (Fisher, 4–8 Mesh, 4Å) to maintain relative humidity conditions below the efflorescence relative humidities of SC and AS near 45% and 40%, respectively (Tang 1996). The aerosol consisting only of absorbing and refractory RB particles and the aerosol consisting only of non-absorbing and non-refractory particles (SC or AS) were initially characterized separately to obtain desired number concentrations and mean sizes, and then these aerosols were combined in a closed stainless steel drum (SKOLNIK, 55 gal) for 0.6 to 20.6 h to allow coagulation of rBC and non-rBC particles. High number concentrations ($\sim 10^5 \text{ cm}^{-3}$) were used to increase coagulation rates. Prior to each experiment, the drum was flushed with particle-free air until the background particle concentration was less than 10 cm^{-3} . The rBC and non-rBC aerosols were continually introduced into the drum for $\sim 1 \text{ h}$ until number concentrations reached steady-state values. The drum was then isolated at both ends, allowing the particle size distributions to evolve via coagulation, wall loss, and

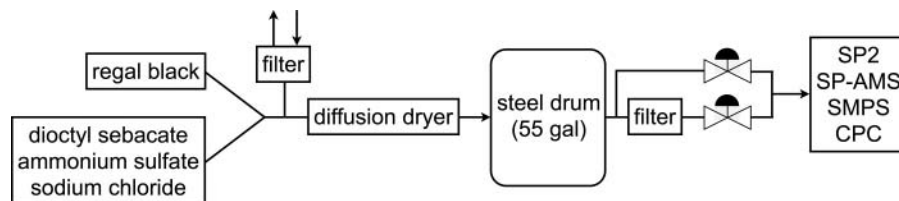


FIG. 1. Experimental setup used to coagulate Regal black (RB) with sodium chloride (SC), ammonium sulfate (AS), and dioctyl sebacate (DOS). Not shown is the coating chamber used for RB→DOS coating experiments.

gravitational sedimentation. Aerosol samples were withdrawn from the drum (and the extracted volume was replaced with filtered air) at intervals to examine changes in particle properties as a function of mixing time (t_{mix}). A HEPA filter diluter placed downstream of the drum before the SP2 reduced the aerosol number concentration by a factor of ~ 100 to minimize particle coincidence during single-particle measurements. Size distributions of rBC number concentrations for particles formed by coagulation of RB and SC measured by the SP2 at various mixing times are shown in Figure 2; the increase in $D_{\text{me,rBC}}$ with increasing time demonstrates that RB+RB coagulation occurred, and thus confirms that the experimental conditions were conducive to coagulation.

In another set of experiments, RB particles were (a) coagulated with drops of dioctyl sebacate (DOS, an organic substance that is liquid at room temperature) generated via homogenous nucleation in a heated flask, and (b) coated with DOS via gas-to-particle condensation, forming RB+DOS and DOS \rightarrow RB particles, respectively. In the coagulation experiments, the techniques and sampling were the same as those used in the previous coagulation experiments with RB and SC or AS. In the condensation experiments, the DOS \rightarrow RB particles were formed by passing RB particles through a chamber with a heated bath containing DOS at various temperatures (103, 107, and 115°C); the dependence of vapor pressure on temperature resulted in different concentrations of DOS vapor and thus different coating thicknesses. The DOS \rightarrow RB particles were sampled directly after leaving the chamber. This set of experiments was conducted to investigate the SP2 responses to particles formed by two different methods that may (at least initially) have different morphologies, i.e., DOS \rightarrow RB particles are expected to have a core-shell configuration, whereas RB+DOS particles will not, at least initially. However, RB may become wetted by the liquid DOS and the coagulated particles may change morphologies (e.g., become more similar to core-shell) over time.

A final set of experiments investigated the dependence of lagtimes on SP2 operating conditions, specifically laser power (qualitatively indicated by laser diode current) and sample flow rate, both of which affect the heating rate of rBC-containing particles. Increasing the pump laser power results in increased intra-cavity laser intensity, and increasing the sample flow rate results in increased particle velocity, both of which lead to a greater rate of energy absorption by the rBC, less time for intra-particle heat transfer from the rBC to the non-rBC material, and thus increased particle heating rate. To examine the relationship between particle velocity and flow rate, the full width at half maximum (FWHM) of the scattering signals from purely scattering NaCl particles was measured at different sample flow rates. As the width of the Gaussian laser beam is independent of the sample flow rate, the inverse of FWHM is directly proportional to the particle velocity, which from Figure 3 is seen to increase linearly with sample flow rate. Two types of experiments were performed. In the first

type, the sample flow rate was held constant and the SP2 laser power was varied by changing the injection current of the pump laser over a range of a factor of 1.5, from 2000 and 3000 mA. In the second type, the laser power was held constant and the sample flow rate was varied over a factor of 4 from 82 to 360 cm³ min⁻¹ by changing the exhaust flow rate while leaving the sheath flow rate constant. All other experiments described in this manuscript were performed with the laser power at 2500 mA and the sample flow rate at 120 cm³ min⁻¹.

RESULTS

Single-Particle SP2 Lagtime Measurements

Several types of single-particle SP2 scattering and incandescence signals were observed during this study, with varying frequency depending on the particle system studied. Examples for RB+SC and RB+DOS particles are shown in Figures 4a–g, respectively. In the first type (Figure 4a), the maximum of the scattering signal occurs before that of the incandescence signal, resulting in a positive lagtime. Under the core-shell assumption, this particle would be interpreted as having an rBC core with sufficient associated non-rBC material that it requires an appreciable time to absorb enough laser energy to evaporate this material. In the second type (Figure 4b), the maxima of the scattering and incandescence signals occur at nearly the same time, resulting in a lagtime of near zero. Such signals are interpreted as resulting from rBC-containing particles with little or no non-rBC material. In the third type (Figure 4c), the maximum of the scattering signal occurs *after* the peak of the incandescence signal, and thus results in a negative lagtime, behavior seemingly inconsistent with the conventional core-shell assumption. SP2 signals with two scattering peaks were also observed; for some of these (Figure 4d) the largest peak occurred before incandescence, whereas for others (Figure 4e) it occurred after incandescence. As the lagtime is defined as the time difference between the peak of the incandescence signal and the maximum value of the scattering signal (regardless of any other features of the scattering signal), these two situations correspond to positive and negative lagtime, respectively. For RB+DOS particles two scattering peaks were also observed, with the smaller one occurring before incandescence and the larger one occurring either simultaneously with (Figure 4f) or after (Figure 4g) incandescence.

Lagtime Distribution Plots

The distributions of lagtimes (derived from the time-dependent SP2 scattering and incandescence signals from individual particles) from each set of coagulation experiments (RB+SC, RB+AS, and RB+DOS) for short (<1 h), intermediate (1.5–2 h), and long (>17 h) mixing times are plotted in Figure 5 as

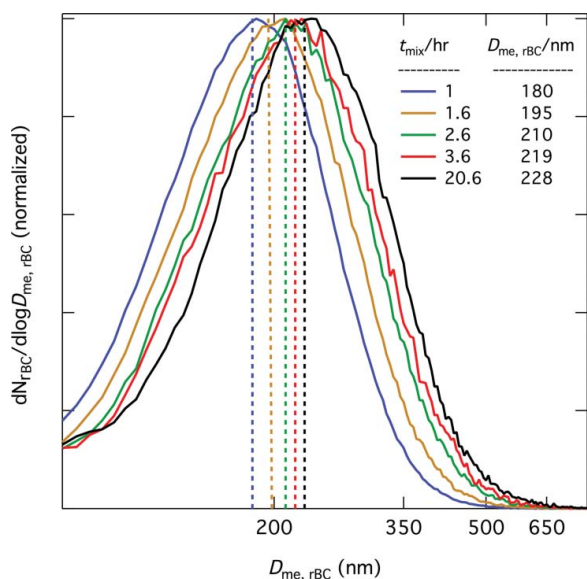


FIG. 2. Size distributions of RB number concentration, $dN_{\text{rBC}}/d\log D_{\text{me,rBC}}$ in terms of mass-equivalent diameter of RB, $D_{\text{me,rBC}}$, measured by the SP2 for different values of mixing time (t_{mix}).

a function of rBC mass-equivalent diameter, $D_{\text{me,rBC}}$. Colors represent the number fraction of particles within given ranges of $\Delta\tau$ (400 ns) and $D_{\text{me,rBC}}$ (5 nm). In each case, the normalized size distribution of RB-number concentration in the representation $dN_{\text{rBC}}/d\log D_{\text{me,rBC}}$ is shown, as is the ratio of the number of particles with positive lagtimes to those with negative lagtimes (positive-to-negative lagtime ratio). Since positive and negative lagtimes only have meaning for rBC particles containing associated non-rBC material, this ratio excludes uncoated rBC particles. As the majority of RB particles remained uncoagulated with SC, AS, or DOS even at the longest mixing time, lagtimes of these particles are not included in the lagtime distribution figures. An RB particle

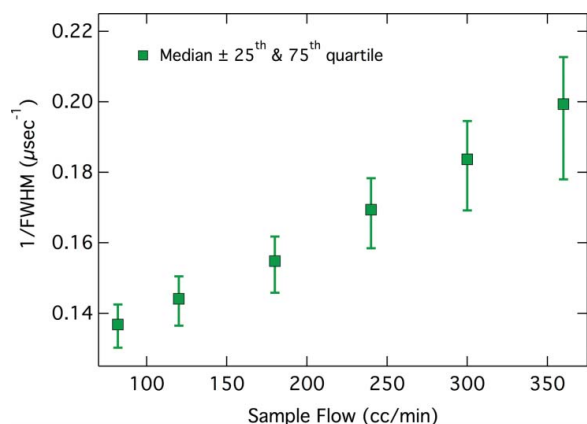


FIG. 3. The inverse of the full width at half maximum (FWHM) for scattering signals from individual NaCl particles as a function of sample flow rate. Each data point is derived from $\sim 15,000$ individual particles.

was assumed to be uncoagulated if it had a value of $\Delta\tau$ in the range -0.4 to $1.2 \mu\text{s}$; this upper limit, although somewhat arbitrary, is commonly accepted in the SP2 research community and allows for uncertainties in instrument response. As particles resulting from coagulation between two or more RB particles will fall in this range, the lagtime distributions presented thus pertain only to particles resulting from coagulation of RB and non-rBC substance.

Coagulation of Regal Black and Sodium Chloride

Lagtime distributions for RB+SC particles are shown in the left column of Figure 5 as a function of $D_{\text{me,rBC}}$ for mixing times ranging from 0.6 h up to 17 h. All these distributions are qualitatively similar and have a prominent mode at small positive lagtimes (near $\sim 1.5 \mu\text{s}$) that extends to larger positive lagtimes at smaller values of $D_{\text{me,rBC}}$, and another mode at negative lagtimes that covers a wider range of values of $\Delta\tau$ (from -1 to $-3 \mu\text{s}$). The location of the maximum value of $D_{\text{me,rBC}}$ for the mode at small positive lagtimes increases with

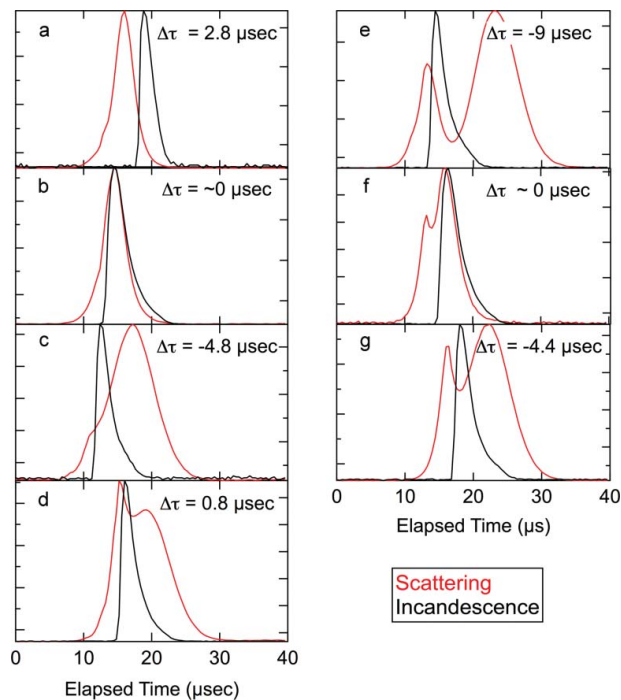


FIG. 4. Examples of scattering and incandescence signals from individual RB+SC (a-e) and RB+DOS (f,g) particles: (a) scattering signal maximum occurs before incandescence signal maximum; (b) scattering signal maximum coincides with incandescence signal maximum; (c) scattering signal maximum occurs after incandescence signal maximum; (d) bimodal scattering signal with scattering signal maximum coincident with incandescence signal maximum and a second scattering peak after incandescence; (e) bimodal scattering signal with scattering signal maximum occurring after incandescence and a second scattering peak before incandescence; (f) bimodal scattering signal with scattering signal maximum coincident with incandescence signal maximum and a second scattering peak before incandescence; and (g) bimodal scattering signal with scattering signal maxima roughly equal in magnitude but opposite distance from the incandescence signal maximum.

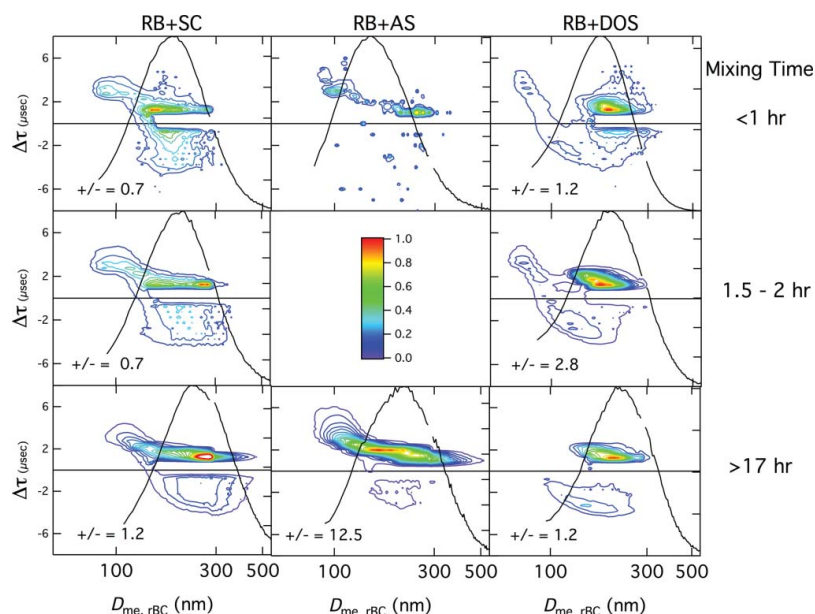


FIG. 5. Lagtime distributions for RB+SC particles (left column), RB+AS particles (center column), and RB+DOS particles (right column) at different mixing times, determined by binning events in ranges of lagtime, $\Delta\tau$ (400 ns) and rBC mass-equivalent diameter, $D_{me, rBC}$ (5 nm). Colors represent the number fraction of particles within given ranges of $\Delta\tau$ and $D_{me, rBC}$. As the majority of RB particles remain uncoagulated, lagtimes of these particles are not included in the figures. Also shown are the normalized size distributions of RB-number concentration, $dN_{rBC}/d\log D_{me, rBC}$, and the positive-to-negative lagtime ratio (number of particles with positive lagtimes to those with negative lagtimes).

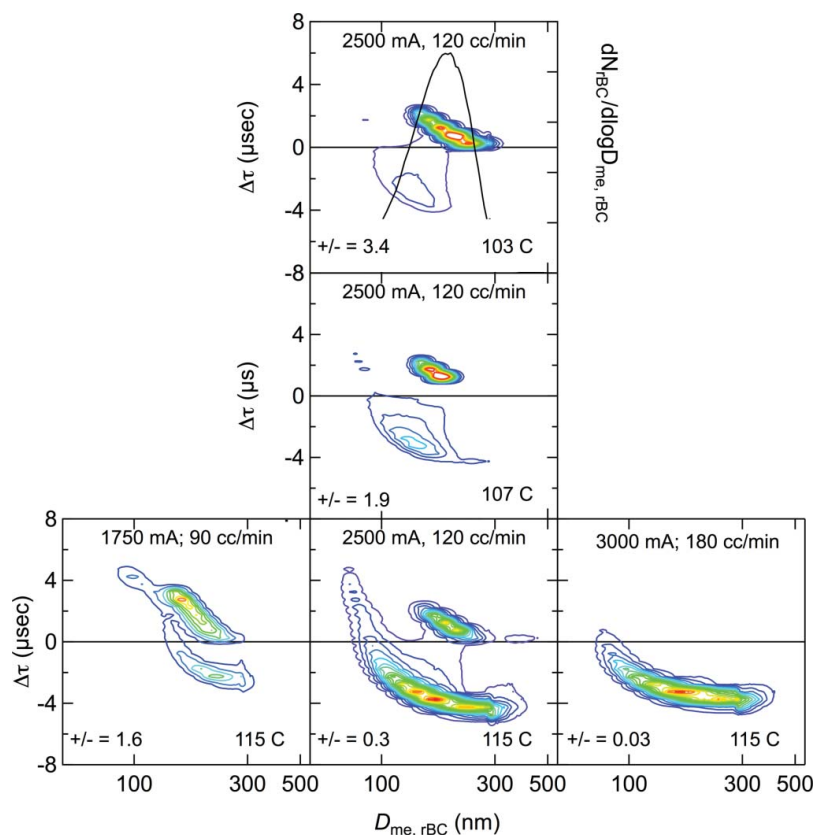


FIG. 6. Lagtime distributions for DOS \rightarrow RB condensation particles at different DOS bath temperatures (middle column) and operating conditions, i.e., sample flow rate and injection laser current, which controls laser power (bottom row). RB-number concentration, $dN_{rBC}/d\log D_{me, rBC}$, the same for all experiments, is shown only in the top central panel. Positive-to-negative lagtime ratios (number of particles with positive lagtimes to those with negative lagtimes) are also shown.

increasing mixing time as a result of coagulation and gravitational settling processes. The most striking observation for the RB+SC system is the presence of both negative and positive lagtimes, which occur in roughly equal numbers (a positive-to-negative lagtime ratio of 0.7 implies that 41% of the lagtimes are positive, and a positive-to-negative ratio of 1.2 implies that 54% of the lagtimes are positive). The occurrence of negative lagtimes is consistent with the original interpretation put forth by Sedlacek et al. (2012) that they originate from the rBC being located at or near the surface, but the presence of positive lagtimes is unexpected for the current situation of coagulated solid–solid particles. Possible reasons for these positive lagtimes will be discussed below.

Coagulation of Regal Black and Ammonium Sulfate

Lagtime distributions for RB+AS particles for mixing times of 1 h and 20.6 h are shown in Figure 5 (middle column). At the shortest mixing times, there are fewer RB+AS coagulated particles than for RB+SC at the shortest mixing time (probably because of differences in the relative distributions of SC, AS, and RB for the different situations), and no positive-to-negative lagtime ratio is presented for this situation. At the longest mixing time, the RB+AS lagtime distribution is qualitatively similar to that for RB+SC at all mixing times and exhibits both positive and negative lagtimes, although the fraction of negative lagtimes for RB+AS particles is substantially smaller than that for RB+SC particles (the positive-to-negative lagtime ratio is 12.5 for RB+AS compared with 1.2 for RB+SC).

Coagulation of Regal Black and Dioctyl Sebacate

Lagtime distributions for RB+DOS particles (Figure 5, right column) also exhibit both negative and positive lagtimes. The distribution for the shortest mixing time is qualitatively similar to those for the RB+SC system at all mixing times (and to that for RB+AS at the longest mixing time); specifically, there is a dominant mode at positive lagtimes centered near $1.5 \mu\text{s}$ distributed over a range of values of $D_{\text{me,rBC}}$, and another, less prominent mode at negative lagtimes distributed over a wide range of lagtimes. In contrast to the RB+SC and RB+AS cases, however, the RB+DOS distribution at the longest mixing time looks qualitatively different and has a second negative lagtime mode centered near $-3.4 \mu\text{s}$ and 150 nm. The RB+DOS lagtime distributions exhibit a greater change with increasing mixing time than do those for RB+SC or RB+AS; the secondary positive lagtime mode at small $D_{\text{me,rBC}}$ values disappears, as does the primary, small magnitude negative lagtime mode.

Scattering signals for individual particles also exhibit significant differences between the RB+DOS and RB+SC cases. For the shortest mixing times, both RB+DOS and RB+SC particles with positive lagtimes exhibit scattering signals similar to that shown in Figure 4a, but for the longest mixing time

the scattering signals from RB+DOS particles exhibit two peaks, either one before incandescence and another coincident with incandescence (Figure 4f), or one before incandescence and another after incandescence (Figure 4g), whereas those from RB+SC particles exhibit only one peak. This will be discussed further below.

Condensation of Dioctyl Sebacate on Regal Black

Lagtime distributions for DOS→RB particles are shown in Figure 6 (middle column) as a function of DOS bath temperature. As the RB size distribution was the same for all bath experiments, $dN_{\text{rBC}}/d\log D_{\text{me,rBC}}$ is shown in only the top panel. In addition, as there were no uncoated RB particles in this study, signals with small lagtimes were not removed from the graphs and analysis, as they were for the coagulation studies. For the sizes of particles and the parameters characterizing the condensation, to good approximation the thickness of the DOS coating would be independent of initial RB diameter and directly proportional to the vapor pressure of DOS, which (based on the values given in O'Hanlon 2003) increases by a factor of ~ 1.4 between 103°C and 107°C , and by a factor of ~ 2 between 107°C and 115°C . However, temperature inhomogeneities in the chamber will result in some spread in the DOS coating thicknesses at any nominal temperature.

DOS→RB particles exhibit both positive and negative lagtimes (Figure 6), but also lagtimes near zero, in spite of the fact that all particles in these condensation experiments were coated and presumably were in a core-shell configuration. The lagtime distributions for DOS→RB particles at the two lower bath temperatures are qualitatively similar to those for RB+DOS at the longest mixing time, but none of the DOS→RB lagtime distributions are similar to any of those for RB+SC or RB+AS particles, or for those for RB+DOS particles at the shortest mixing times. Specifically, DOS→RB negative lagtime distributions do not exhibit the small lagtime mode (lagtimes near $1 \mu\text{s}$ and $D_{\text{me,rBC}}$ between 200 nm and 300 nm) observed for these other particles. The DOS→RB lagtime distributions contain two distinct modes for all bath temperatures, one at positive values of $\Delta\tau$ and another at negative values. With increasing DOS coating thickness (increasing bath temperature), there is a large shift in the distribution from the positive mode to the negative mode (positive-to-negative lagtime ratio decreasing from 3.4 at 103°C to 0.3 at 115°C), with the lagtimes changing from positive to negative without taking intermediate values. A similar increase in negative lagtimes with increasing coating thickness was reported by Moteki and Kondo (2007).

Dependence of Lagtime Distributions on SP2 Operating Conditions

Lagtime distributions for RB+SC particles in which laser power and sample flow rate were varied are shown in Figure 7,

with laser power increasing from top (2000 mA) to bottom (3000 mA) and sample flow rate increasing from left to right (82, 120, and 240 cm³ min⁻¹). At the lowest laser power and sample flow rate considered (2000 mA and 82 cm³ min⁻¹), the lagtimes are predominantly positive (positive-to-negative lagtime ratio 6.1), behavior that would be typically ascribed to a core-shell configuration (Figure 7a). With increasing sample flow rate at this same laser power (Figures 7b and c), the shapes of the lagtime distributions at positive lagtimes remain qualitatively similar, but a mode begins to appear at negative lagtimes concomitant with a decrease in the positive-to-negative lagtime ratio. Likewise, with increasing sample flow rate at a laser power of 3000 mA, the shapes of the lagtime distributions at positive lagtimes are qualitatively similar to each other (Figures 4d–f), with a maximum remaining unchanged near $D_{\text{me,rBC}} = 290$ nm, but there is an increase in the frequency of occurrence of negative lagtimes, which eventually dominate over positive lagtimes. At a given sample flow rate, the lagtime distributions at higher laser power (3000 mA) are qualitatively similar to those at lower laser power (2000 mA) but exhibit large increases in the number of particles with negative lagtimes (and correspondingly large decreases in the positive-to-negative lagtime ratios). The mean values of negative lagtimes are also larger.

The results of these experiments are also summarized in Figure 8, which encompasses a wider array of conditions than shown in Figure 7. There is a systematic decrease in the positive-to-negative lagtime ratio with either increased laser power or increased sample flow rate, both of which increase particle heating rate. Over the range of SP2 laser powers and sample flow rates examined, the laser power exerts a much larger influence on lagtime distributions than does the sample flow rate.

Lagtime distributions for DOS→RB particles under different laser powers and sample flow rates, but at the same bath temperature (and thus coating thickness), are shown in the bottom row of Figure 6. With increased particle heating rate (left to right), the positive lagtime mode essentially disappears and is replaced by a negative lagtime mode, and the positive-to-negative lagtime ratio decreases from 1.6 to 0.03.

DISCUSSION

Single-Particle Energy Balance in the SP2

The behavior of an rBC-containing particle in the SP2 is determined by both the rate at which the rBC absorbs energy from the laser and the rate at which this energy is dissipated (Moteki and Kondo 2007). This dissipation occurs primarily through conduction to the non-rBC material, from which the energy is subsequently removed through heating and evaporation (i.e., latent heat) of this substance and through conduction to the surrounding gas. The rates of energy absorption and dissipation depend on several factors, the most fundamental of

which are the masses and configuration of the rBC and non-rBC components (e.g., core-shell vs. on surface). These determine the absorption cross section and thus the rate at which the particle absorbs incident radiation, and they also govern the rate of intra-particle heat dissipation and the rate of heat conduction to the surrounding gas. This dissipation can be so rapid for particles with a sufficiently small BC mass that these particles never incandesce, and thus will not be detected by the SP2. This effect explains the small particle size limit for SP2 incandescence detection (Schwarz et al. 2010), and it also explains the increased number of lagtimes observed for particles with smaller $D_{\text{me,rBC}}$ under higher laser power condition (Figure 7, bottom row).

The primary factors that affect the rate at which a given rBC-containing particle absorbs energy are the SP2 operating conditions, specifically the laser power, which determines light intensity at a given location, and the sample flow rate, which governs the speed of the rBC particles through the laser. The effects of these instrument operating conditions on the positive-to-negative lagtime ratio are shown in Figures 7 and 8. Under low laser power and low sample flow rate, the rate at which energy is absorbed by the rBC is relatively slow, and much of the energy can be transferred to and through the non-absorbing, non-refractory substance, evaporating most or all of this substance before the rBC attains its sublimation temperature, and resulting in a positive lagtime. Conversely, under sufficiently high laser power and sample flow rate, the rate at which energy is absorbed by the rBC may be so high that this energy cannot be transferred to and through the non-rBC substance before some of this substance evaporates at the interface between the non-rBC and rBC. Depending on the extent of this evaporation and on the morphology of the particle, the non-rBC and rBC components can separate, with some of the separated non-rBC material continuing through the SP2 laser as a pure scatterer. Such a situation could result in either a positive or negative lagtime (e.g., Figures 4d and e), depending on the amount of this remaining material. This mechanism was proposed by Moteki and Kondo (2007) for the observation of negative lagtimes observed for thickly coated rBC-containing particles in a core-shell-like configuration, and might also explain the results shown in Figure 6.

The primary factors that affect the intra-particle heat dissipation rate and the subsequent evaporation of the non-rBC component for a given rBC-containing particle are the thermochemical properties of this non-rBC substance (e.g., thermal diffusivity, specific heat, latent heat, etc.) and the extent of contact between the rBC and non-rBC substances. Evidence for the importance of the non-rBC thermochemical properties is the observed difference in behavior between RB+SC and RB+AS particles. In spite of the fact that both of these systems represent solid–solid coagulation, the latter exhibits a much higher fraction of positive lagtimes (Figure 5), likely reflecting the greater thermal volatility of AS compared with SC. Evidence for the importance of the extent of contact

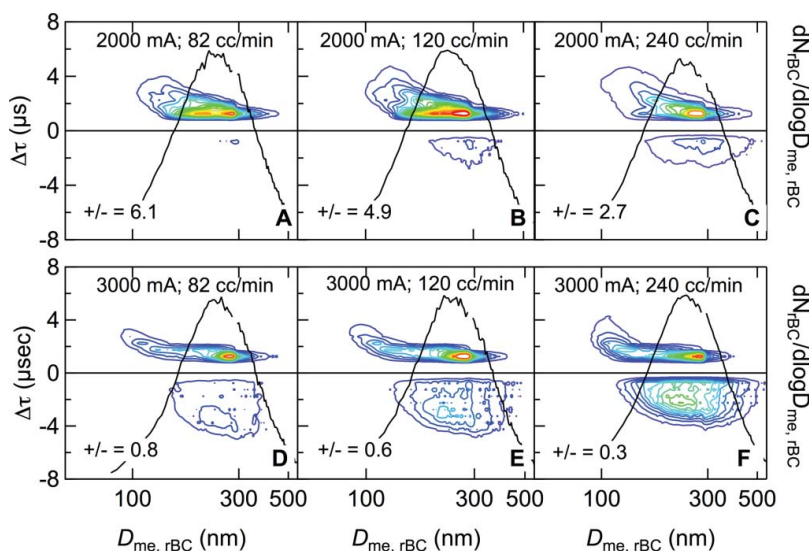


FIG. 7. Dependence of RB+SC lagtime distributions on SP2 operating conditions, i.e., sample flow rate (increasing left to right) and injection laser current, which controls laser power (top row: 2000 mA, bottom row: 3000 mA). Also shown are the normalized size distributions of RB-number concentration, $dN_{rBC}/d\log D_{me, rBC}$, and the positive-to-negative lagtime ratio (number of particles with positive lagtimes to those with negative lagtimes).

between the rBC and non-rBC components is provided by comparison of lagtime distributions for the coagulated RB+DOS particles at the shortest mixing times (Figure 5, upper right panel) and the condensed DOS→RB particles (Figure 6, top panel, which has the same SP2 operating conditions); the former has a much lower positive-to-negative ratio, probably due to the particles in this system having much less physical and thus thermal contact between DOS and RB.

It is the balance between these rates of energy absorption and energy dissipation that determines the lagtime for a given rBC-containing particle. As such a particle moves through the SP2, it initially scatters light, but this scattering signal attains a maximum value that is determined by the competing effects

of a decreasing scattering cross section resulting from particle evaporation and the increasing laser light intensity as the particle moves further into the laser beam. If the non-rBC substance evaporates completely, this scattering maxima will occur before (or at) incandescence, resulting in a positive (or zero) lagtime. However, if the non-rBC and rBC components separate, then the separated non-rBC particle (or particles) will pass through laser beam as a pure scatterer, with its (their) scattering cross section(s) remaining constant. The resulting

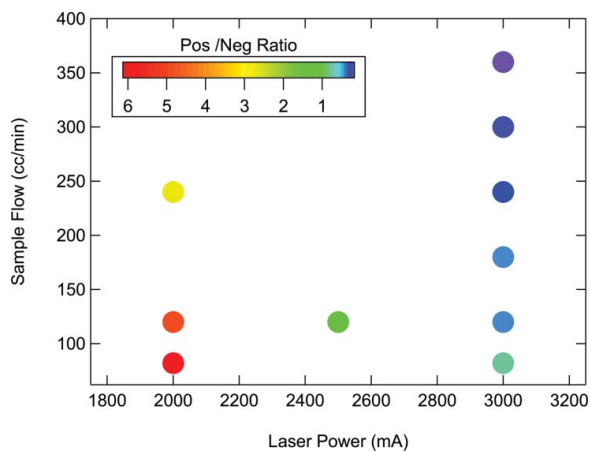


FIG. 8. Dependence of positive-to-negative lagtime ratio (number of particles with positive lagtimes to those with negative lagtimes) on SP2 operating conditions, i.e., sample flow rate and injection laser current, which controls laser power.

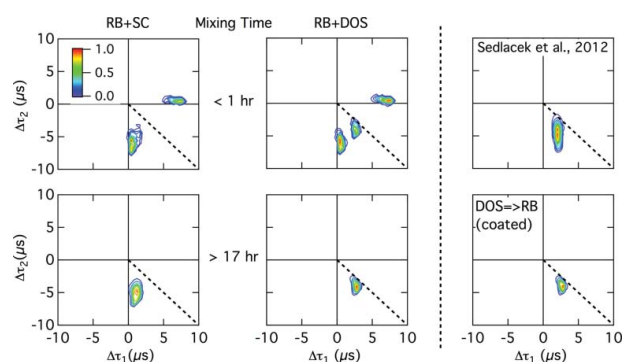


FIG. 9. Distributions of $\Delta\tau_1$ (difference between the time of the maximum of the incandescence signal and that of the first maximum of the scattering signal) and $\Delta\tau_2$ (difference between the time of the maximum of the incandescence signal and that of the second scattering maximum) for bimodal scattering signals from RB+SC (left column) and RB+DOS (center column) particles, at the shortest (top panels in each column) and longest (bottom panels) mixing times. Right column contains distributions for ambient particles from Sedlacek et al. (2012) (top panel) and from bimodal scattering distributions for RB→DOS particles (lower panel). Color represents the number fraction of particles in given ranges of $\Delta\tau_1$ and $\Delta\tau_2$. Dotted line bisecting the lower right quadrant of each plot denotes where the first and second scattering peaks are equidistant (temporally) from the incandescence peak.

scattering signals for each of the separated, non-absorbing particles will be Gaussian, following that of the laser intensity, with maxima at times when the particles are at the center of the laser (where the intensity is greatest). In contrast, the initial scattering maximum will be non-Gaussian. As the lagtime is defined as the difference between the time of the peak of the abrupt incandescence of the rBC and the time of the largest value of the scattering signal, a separated particle could have either a positive or a negative lagtime, depending on the relative magnitudes of the scattering maxima. Thus, two situations that are qualitatively very similar could be classified as quantitatively very different.

Lagtimes of Individual Particles

This laboratory investigation explicitly demonstrates that both positive and negative lagtimes can result from particles formed by the coagulation of two solid particles, the coagulation of a solid particle and a liquid droplet, and the condensation of liquid material on a solid particle. Thus, attempts to infer particle morphology from lagtimes alone must be undertaken with extreme caution. In particular, interpretations of lagtime observations based on the assumption of core-shell particle configurations must be regarded with considerable suspicion. In addition, negative lagtimes were observed for each particle type, and accounted for at least 10% of the rBC particles sampled for each experiment, from which it must be concluded that such lagtimes do not correspond to anomalies, but are expected for these and presumably other types of BC-containing particles. For example, Sedlacek et al. (2012) also observed negative lagtimes for $\sim 10\%$ of ambient BC-containing particles under background conditions when biomass burning plumes were not present, and similar values were reported by Moteki et al. (2014) for ambient urban particles. Finally, a substantial fraction of particles in each experiment exhibited scattering signals with two maxima, and as discussed above, such a signal may correspond to either a positive or a negative lagtime, depending on the relative magnitudes of these maxima (Figure 4). As noted above, the magnitudes, and even the sign, of the lagtime are not intrinsic properties of an rBC-containing particle but depend on the rates of energy absorption and dissipation, and thus on SP2 operating conditions.

Lagtime Distributions

Two distinct patterns are observed for lagtime distributions in these experiments. The first pattern contains three modes: one with rather small positive values of $\Delta\tau$ extending over a range of values of $D_{\text{me,rBC}}$; a second, smaller, mode at larger positive values of $\Delta\tau$ at small values of $D_{\text{me,rBC}}$; and a third mode extending over a wider range of negative values of $\Delta\tau$ (Figure 5, except lower right panel; Figure 7). This first pattern was observed for RB+SC and RB+AS particles at all mixing times, and for RB+DOS particles at the shorter two

mixing times. The second pattern consists of a mode with positive values of $\Delta\tau$ increasing with decreasing $D_{\text{me,rBC}}$, or a mode with negative values of $\Delta\tau$, the magnitude of which decreases with decreasing $D_{\text{me,rBC}}$ and sometimes extends to positive values of $\Delta\tau$, or both (Figure 6 and the lower right panel of Figure 5). This second pattern was observed for DOS \rightarrow RB particles and for RB+DOS particles at the longest mixing times.

The similarity between the lagtime distributions observed for the RB+DOS particles at the shortest mixing times (Figure 5, upper two panels in right column) and that for RB+SC at all mixing times (best seen in Figure 5 in the lower left panel) suggests that the DOS initially had limited contact with the RB and that the two components could easily separate under the operating conditions of this study. The similarity between the lagtime distributions observed for the RB+DOS particles at the longest mixing time (Figure 5, lower right panel) and that for DOS \rightarrow RB at the lower bath temperatures (top and middle panels of Figure 6), however, suggests that with sufficient time, the liquid DOS (in the RB+DOS coagulated particles) wets the RB surface and eventually completely encapsulates it, resulting in a core-shell-like structure similar to that expected for DOS \rightarrow RB, but not possible for RB+SC particles. This wetting also results in increased physical, and thus thermal, contact between the two substances. RB contains oxidized surfaces and is collapsed in water, and thus possesses the chemical and physical properties favorable for wetting by DOS. Such a core-shell-like structure is consistent with the results observed for the lagtime behavior of individual particles discussed above. Both RB+DOS particles at the shortest mixing times and RB+SC particles with positive lagtimes exhibit scattering signals with a single maximum, similar to the example in Figure 4a, whereas the scattering signals from RB+DOS particles at the longest mixing times exhibit two peaks, either one before incandescence and another coincident with incandescence (Figure 4f), or one before incandescence and another after incandescence (Figure 4g). Scattering signals having two maxima are discussed further below.

The DOS \rightarrow RB particles, in which the rBC is expected to be completely coated with DOS in a core-shell-like configurations, and which thus have extensive thermal contact between the rBC and non-rBC components, exhibit both positive and negative lagtimes (Figure 6). The fact that the majority of such particles at the lower bath temperatures (i.e., those with thinner coatings) exhibit positive lagtimes is likely due to the complete evaporation of the DOS before incandescence of the rBC. The trend of decreasing values of positive lagtimes with increasing $D_{\text{me,rBC}}$ can be explained by the fact that for a given DOS bath temperature, the coating thickness is nearly the same for all particles, as noted above. With increasing $D_{\text{me,rBC}}$ there is greater energy absorbed per mass of DOS coating, and thus this coating can be evaporated more quickly, resulting in lower positive values of $\Delta\tau$. The existence of negative lagtimes can be explained by some fraction of the particles

having coatings so thick that the RB is unable to transfer heat sufficiently rapidly, resulting in fragmentation, as observed in laboratory settings by Moteki and Kondo (2007). The trend in negative lagtime values with decreasing $D_{\text{me,rBC}}$, especially at the smallest particle sizes (lowest $D_{\text{me,rBC}}$), can be explained by the increasing dissipation of heat to the gas via conduction, which will decrease the particle heating rate, enabling more coating material to evaporate, thereby decreasing fragmentation.

Bimodal Scattering Distributions

As introduced above, the current operating definition of lagtime utilizes only the scattering peak with the largest maximum. However, as a large fraction of rBC-containing particles exhibit bimodal scattering signals, it is worth examining whether these signals offer utility in studying rBC-containing morphology. To this end, distributions of $\Delta\tau_2$, defined as the difference between the time of the maximum of the incandescence signal and that of the second maximum of the scattering signal, and $\Delta\tau_1$, defined as the difference between the time of the maximum of the incandescence signal and that of the first scattering maximum, are shown in Figure 9. For a bimodal scattering signal, $\Delta\tau_1$ will always be greater than or equal to zero (as the first scattering maximum will always occur before or simultaneous to incandescence), and the lagtime will be equal to either $\Delta\tau_1$ or $\Delta\tau_2$, depending on which scattering maximum is larger.

The distributions of $\Delta\tau_1$ and $\Delta\tau_2$ for RB+SC and RB+DOS particles at the shortest (<1 h) mixing times are similar (as were the lagtime distributions for these particles), although the distribution for the RB+DOS particles contains one more cluster than that for RB+SC particles. Both contain a dominant cluster near $\Delta\tau_1 = 0.4 \mu\text{s}$ and $\Delta\tau_2 = -6 \mu\text{s}$ and a secondary cluster near $\Delta\tau_1 = 7 \mu\text{s}$ and $\Delta\tau_2 = 0.4 \mu\text{s}$, but the distribution for RB+DOS particles has a less populated cluster near the bisecting line ($\Delta\tau_1 = -3 \mu\text{s}$ and $\Delta\tau_2 = -4 \mu\text{s}$), indicating that these bimodal scattering signals are more nearly symmetric about the incandescence signal. In contrast, the distributions for both types of particles at the longest mixing time each consist of only a single cluster, but these are in different locations; that for RB+SC is near the dominant cluster that occurred at short mixing times for these particles, whereas that for RB+DOS particles is near the less populated one for shorter mixing times that occurred near the bisecting line. The loss of the cluster that was located near $\Delta\tau_1 = \sim 7 \mu\text{s}$ and $\Delta\tau_2 = 0.4 \mu\text{s}$ in both the RB+SC and RB+DOS distributions at short times is ascribed to the loss of particles through gravitational sedimentation, as these particles were characterized by large RB components. This latter distribution is nearly identical to that for RB→DOS particles (Figure 9, right column, lower panel), further supporting the argument presented above that the morphologies of

RB+DOS particles at the longest mixing times and of DOS→RB particles are similar.

Implications for Ambient Observations

The SP2 lagtime distribution observed by Sedlacek et al. (2012) for an air mass containing aged biomass-burn tracers (Figure 4 in Sedlacek et al. 2012), which was obtained with the same SP2 instrument operating at the same conditions as the current laboratory investigation (laser power 3000 mA and sample flow rate $120 \text{ cm}^3 \text{ min}^{-1}$), is qualitatively more similar to the second lagtime distribution pattern discussed above (i.e., for RB+DOS particles at longer mixing times and for DOS→RB particles) than the first pattern (i.e., for RB+SC and RB+AS particles and for RB+DOS particles at the shorter two mixing times). This is especially so for the dependence of the mode at negative lagtimes on $D_{\text{me,rBC}}$. The biomass burning plume observed by Sedlacek et al. (2012) exhibited a lagtime distribution with three prominent modes: one centered at large positive lagtimes at small values of $D_{\text{me,rBC}}$, one at small positive lagtimes at larger values of $D_{\text{me,rBC}}$, and one at negative lagtimes with increasingly larger negative values with increasing values of $D_{\text{me,rBC}}$. There was no evidence in the ambient biomass burning observations of a negative lagtime mode comprised of small negative values of $\Delta\tau$ at larger $D_{\text{me,rBC}}$, which has been found to dominate the lagtime distribution observed for the RB+SC system. The background ambient observations reported by Sedlacek et al. (2012) always exhibited measurable negative lagtimes, averaging $\sim 10\%$ of the total number of rBC-containing particles (not just those exclusive of the range of $\Delta\tau$ of 0.4 to $1.2 \mu\text{s}$). In addition, the distribution of $\Delta\tau_1$ and $\Delta\tau_2$ for the ambient particles analyzed by Sedlacek et al. (2012) that have two scattering signals, shown in Figure 9 (right column, upper panel), is similar to that for RB+DOS particles at the longest mixing time and to that for DOS→RB particles, although it extends over a wider range of values of $\Delta\tau_2$, possibly reflecting different values of $D_{\text{me,rBC}}$ and/or different thermochemical properties for these particles.

The similarity in the lagtime distributions and the distributions of $\Delta\tau_1$ and $\Delta\tau_2$ for the particles observed in the aged biomass burning plume and those of the laboratory RB+DOS and DOS→RB particles suggests that the particles in the biomass burning plume had extensive contact between the rBC and non-rBC components. There are several morphologies that would allow for this. For rBC that has collapsed into a nearly spherical shape (as in the current laboratory investigation), one such morphology is complete encapsulation by the non-rBC substance, as would be expected for the DOS→RB particles – whether in a core-shell or off-center (eccentric) configurations. However, if the rBC retained a fractal-like structure, as is typical for nascent soot in the atmosphere, then a morphology that would allow for extensive thermal contact is one in which the rBC is on the surface (as suggested by Sedlacek

et al. [2012]) and is similar to an octopus (as a surrogate for the fractal-like nascent soot) holding onto a rock (as a surrogate for the non-rBC substance) with its tentacles. The current results further suggest that the differences between the ambient background particles and the biomass burning particles observed by Sedlacek et al. (2012) were due to different morphologies and/or different thermochemical properties of the non-rBC material. Although the specific morphology of these particles cannot be positively identified using the SP2 lagtime approach, the observations may provide useful information on source attribution and population-based mixing state for biomass particles.

As discussed earlier, Moteki and co-workers (2014) have developed a mixing-state analysis methodology based on the behavior of time-dependent scattering cross section at the onset of rBC incandescence. Our results suggest that the operating conditions of the SP2 (laser power and sample flow rate), the thermochemical properties of the non-rBC material, and the contact between the non-rBC and rBC will affect the temporal behavior of the scattering cross section between non-refractory sublimation and rBC incandescence, the timeframe considered by Moteki et al. (2014). For example, a lower heating rate imposed on a coagulated rBC particle – as would occur if the sample flow rate was reduced – would increase the likelihood of sublimation of the non-refractory material. This could lead to a condition that more closely mimics the observed behavior ascribed to core-shell configurations by exhibiting material evaporation well before rBC incandescence.

In situations with high rBC particle number concentrations, such as biomass burning plumes, reduction of the sample flow rate to minimize the effects of coincidence counting will decrease particle heating rate and will likely change the response of the rBC-containing particle in the SP2. Future analysis using the present data set will specifically examine the effects of SP2 operating conditions on the Moteki mixing state analysis in an effort to better map out the performance envelope of this analysis methodology.

CONCLUSIONS

This study demonstrates and highlights several important aspects related to the behavior of rBC-containing particles in the SP2, specifically particle fragmentation, which is important for lagtime analyses and may also be important for other analyses: (1) SP2 operating conditions affect the frequency of particle fragmentation; (2) the physical and chemical properties of rBC-containing particles affect the frequency of fragmentation; and (3) the SP2 appears to fragment a substantial fraction of rBC-containing particles under most operating conditions.

At this point, it is worth examining the utility of lagtimes and lagtime distributions for making inferences about the morphologies and thermochemical properties of rBC-containing particles. From our results, we offer the following observations. First, two different general lagtime distribution patterns

were observed in these experiments: one resulting from coagulation of RB with either solid SC or solid AS, or with liquid DOS at short mixing times, and the other resulting from condensation of liquid DOS onto RB or from coagulation of RB with liquid DOS particles at longer mixing times. These different lagtime distributions are attributed to different particle morphologies. The dependence of the lagtime distribution of coagulated RB+DOS particles on mixing time can be explained by wetting of RB by the DOS, with the lagtime distribution (and the morphology of the particles) changing from being similar to that for RB+SC particles to becoming more similar to that for DOS→RB particles.

Second, this study demonstrates the dominant role played by SP2 operating conditions, specifically laser power and sample flow rate, in determining the observed lagtime distributions. These operating conditions influence the rates of laser heat uptake and internal particle heat transfer (and dissipation) within rBC-containing particles, which in turn affect the fraction of particles that fragment in the SP2 laser and generate negative lagtimes in particular, and the observed lagtime distributions in general. The effects of operating conditions are shown explicitly for coagulated RB+SC and RB+AS particles and for DOS→RB particles. In all cases, the positive-to-negative lagtime ratio is shown to be dependent upon these conditions: lower (higher) laser power and lower (higher) sample flow rate generates slower (faster) particle heating and higher (lower) positive-to-negative lagtime ratios. Comparison of lagtime results between different studies with different SP2 instrument parameters will therefore be challenging at best, and to enable meaningful comparisons and to further analyses of SP2 measurements, it is imperative that SP2 laser power and sample flow rate be reported for all future studies. The best practice for quantifying laser power is to measure the scattered light from a standard particle (Schwarz et al., 2010), and the best practice for quantifying particle velocities is to measure the transit times (e.g., FWHM) for non-absorbing particles passing through the laser beam (Schwarz et al. 2015), both of which can be readily accomplished using the same standard particles (e.g., 220-nm PSL).

Third, for given SP2 operating conditions, lagtime distributions are also dependent on the thermochemical properties of the non-rBC substance. Comparison of lagtime distributions for coagulated RB+SC and RB+AS particles reveals measurable differences in behavior (e.g., RB+AS particles consistently generated higher positive-to-negative lagtime ratios), which are attributed to the greater thermal volatility of AS than that of SC.

Fourth, all particle morphologies and compositions examined here, whether the rBC was on the surface (e.g., RB+SC) or inside the particle (e.g., DOS→RB), exhibited both positive and negative lagtimes. Such a result can confound lagtime-based mixing-state analyses, even those involving examination of individual particle signals. As positive lagtimes from particles with rBC on the surface can mimic those from particles

with core-shell configurations in all aspects, it is not possible to attribute positive lagtimes to a core-shell configuration. Such an attribution could lead to erroneous conclusions, including those regarding radiative properties (especially absorption). The concept of coating thickness for such particles, as is typically obtained from signal scattering and incandescence amplitudes with the implicit assumption of a core-shell configuration, would (of course) be meaningless.

Fifth, the mere presence of a negative lagtime cannot be used to infer particle morphology, as both solid–solid particles and core-shell particles with thick coatings can exhibit negative lagtimes. In this regard, the conclusions of Dahlkötter et al. (2014) that negative lagtimes result only from thickly coated particles in a core-shell configuration is not supported by our observations. The SP2 technique appears to fragment a substantial fraction of rBC-containing particles under most operating conditions, both under ambient conditions and in laboratory experiments.

Sixth, although the current results indicate that SP2 lagtime analysis is not able to unambiguously determine particle morphology or to provide information on the thermochemical properties of the non-rBC component directly, the lagtime distribution observations may provide useful information on source attribution and population-based mixing states for rBC-particle populations with different lagtime characteristics. For example, the observations reported by Sedlacek et al. (2012) of two types of rBC-containing particles defined by their lagtime differences, using the same instrument with constant operating conditions, were highly correlated with ambient background particles and tracers of biomass burning transported over the sampling site. In addition, the strong dependence of the magnitudes and signs of lagtimes on SP2 operating conditions might be exploited to probe rBC-containing particles for additional information. For example, the laser power could be modulated for times that would be sufficiently long to yield good statistics but sufficiently short that properties of the aerosol sampled would remain constant.

Finally, both positive and negative lagtimes may derive from bimodal light scattering signals (Figures 4c–f), a subtlety not appreciated by the current definition of lagtime. The lagtime methodology reduces the measured scattering and incandescence signals for each rBC-containing particle to a single quantity, which cannot account for bimodal scattering signals nor can it unambiguously discriminate between effects due to SP2 operating conditions or varying rBC chemical and physical properties. Similarly, the two measured quantities employed by Moteki et al. (2014) would also be expected to be sensitive to the operating conditions. Future work will investigate the full scattering and incandescence signals of individual particles (e.g., Figure 9) and their sensitivities to details of particle morphology and thermochemical properties with the goal of identifying meaningful quantities that are insensitive to the SP2 operating conditions.

ACKNOWLEDGMENTS

Researchers thank the DOE Atmospheric Radiation Measurement (ARM) Climate Research Facility for the use of the Single-Particle Soot Photometer (SP2).

FUNDING

This research was performed under sponsorship of the US DOE Office of Biological & Environmental Sciences (OBER) Atmospheric Research Program (ASR) under contracts DE-AC02-98-CH10886 (BNL), DE-SC0006980 (Boston College), DE-FG02-05ER63995 (ARI) NSF Award Numbers ATM-0854916 and 1244918 (Boston College), and EPA STAR grant No. 83503301 (Boston College).

REFERENCES

- Bond, T. C., Doherty, S. J., Fahey, D. W., Forster, P. M., Berntsen, T., DeAngelo, B. J., Flanner, M. G., Ghan, S., Kärcher, B., Koch, D., Kinne, S., Kondo, Y., Quinn, P. K., Sarofim, M. C., Schultz, M. G., Schulz, M., Venkataraman, C., Zhang, H., Zhang, S., Bellouin, N., Guttikunda, S. K., Hopke, P. K., Jacobson, M. Z., Kaiser, J. W., Klimont, Z., Lohmann, U., Schwarz, J. P., Shindler, D., Storelvmo, T., Warren, S. G., and Zender, C. S. (2013). Bounding the Role of Black Carbon in the Climate System: A Scientific Assessment. *J. Geophys. Res.*, 118. doi:10.1002/jgrd.50171.
- Dahlkötter, F., Gysel, M., Sauer, D., Minikin, A., Baumann, R., Seifert, P., Ansmann, A., Fromm, M., Voigt, C., and Weinzierl, B. (2014). The Pagami Creek Smoke Plume After Long-Range Transport to the Upper Troposphere over Europe – Aerosol Properties and Black Carbon Mixing State. *Atmos. Chem. Phys.*, 14:6111–6137. doi:10.5194/acp-14-6111-2014.
- Gao, R. S., Schwartz, J. P., Kelly, K. K., Fahey, D. W., Watts, L. A., Thompson, T. L., Spackman, J. R., Slowik, J. G., Cross, E. S., Han, J.-H., Davidovits, P., Onasch, T. B., and Worsnop, D. R. (2007). A Novel Method for Estimating Light-Scattering Properties of Soot Aerosols Using a Modified Single-Particle Soot Photometer. *Aerosol Sci. Technol.*, 41:125–135. doi:10.1080/02786820601118398.
- Moteki, N., and Kondo, Y. (2007). Effects of Mixing State on Black Carbon Measurements by Laser-Induced Incandescence. *Aerosol Sci. Technol.*, 41:4. 398–417. doi:10.1080/02786820701199728.
- Moteki, N., and Kondo, Y. (2008). Method to Measure Time-Dependent Scattering Cross-Sections of Particles Evaporating in a Laser Beam. *J. Aerosol Sci.*, 39:348–364. doi:10.1029/2006JD007076.
- Moteki, N., Kondo, Y., and Adachi, K. (2014). Identification by Single-Particle Soot Photometer of Black Carbon Particles Attached to Other Particles: Laboratory and Ground Observations in Tokyo. *J. Geophys. Res.*, 119:1031–1043. doi:10.1002/2013JD020655.
- O’Hanlon, J. F. (2003). *A User’s Guide to Vacuum Technology*, 3rd Edn. John Wiley, New York, NY, 516 pp.
- Ramanathan, V., and Carmichael, G. (2008). Global and Regional Climate Changes Due to Black Carbon. *Nature Geosci.*, 1:221–227.
- Schwarz, J. P., Goa, R. S., Fahey, D. W., Thomson, D. S., Watts, L. A., Wilson, J. C., Reeves, J. M., Darbeheshti, M., Baumgardner, D. G., Kok, G. L., Chung, S. H., Schulz, M., Hendricks, J., Lauer, A., Kärcher, B., Slowik, J. G., Rosenlof, K. H., Thompson, T. L., Langford, A. O., Loevenstein, M., and Aikin, K. C. (2006). Single-Particle Measurements of Midlatitude Black Carbon and Light-Scattering Aerosols from the Boundary Layer to the Lower Stratosphere. *J. Geophys. Res.*, 111:D16207. doi:10.1029/2006JD007076.
- Schwarz, J. P., Spackman, J. R., Fahey, D. W., Gao, R. S., Lohmann, U., Stier, P., Watts, L. A., Thomson, D. S., Lack, D. A., Pfister, L., Mahoney, M. J.,

- Baumgardner, D., Wilson, J. C., and Reeves, J. M. (2008). Coatings and Their Enhancement of Black Carbon Light Absorption in the Tropical Atmosphere. *J. Geophys. Res.*, 113:D03203. doi:10.1029/2007JD009042.
- Schwarz, J. P., Spackman, J. R., Gao, R. S., Perring, A. E., Cross, E., Onasch, T. B., Ahern, A., Wrobel, W., Davidovits, P., Olfert, J., Dubey, M. K., Massoleni, C., and Fahey, D. W. (2010). The Detection Efficiency of the Single Particle Soot Photometer. *Aerosol Sci. Technol.*, 44:612–628. doi:10.1080/02786826.2010.481298.
- Schwarz, J. P., Perring, A. E., Markovic, M. Z., Gao, R. S., Ohata, S., Langridge, J., Law, D., McLaughlin, R., and Fahey, D. W. (2015). Technique and Theoretical Approach for Quantifying the Hygroscopicity of Black-Carbon-Containing Aerosol Using a Single Particle Soot Photometer. *J. Aerosol Sci.*, 81:110–126. doi:10.1016/j.jaerosci.2014.11.009.
- Sedlacek, A. J., Lewis, E. R., Kleinman, L., Xu, J., and Zhang, Q. (2012). Determination of and Evidence for Non-Core-Shell Structure of Particles Containing Black Carbon Using the Single-Particle Soot Photometer (SP2). *Geophys. Res. Lett.*, 39. doi:10.1029/2012GL050905.
- Subramanian, R., Kok, G. L., Baumgardner, D., Clarke, A., Shinozuka, Y., Campos, T. L., Heizer, C. G., Stephens, B. B., de Foy, B., Voss, P. B., and Zaveri, R. A. (2010). Black Carbon Over Mexico: The Effect of Atmospheric Transport on Mixing State, Mass Absorption Cross-Section, and BC/CO Ratios. *Atmos. Chem. Phys.*, 10:219–237. doi:10/5194/acp-10-209-2010.
- Tang, I. N. (1996). Chemical and Size Effects of Hygroscopic Aerosols on Light Scattering Coefficients. *J. Geophys. Res.*, 101, D14:19245–19250.